Journal of the Meteorological Society of Japan, Vol. 87, No. 5, pp. 895–912, 2009.
DOI:10.2151/jmsj.87.895

Development of an Improved Turbulence Closure Model for the Atmospheric Boundary Layer

Mikio NAKANISHI

Department of Earth and Ocean Sciences, National Defense Academy, Yokosuka, Japan

and

Hiroshi NIINO

Ocean Research Institute, The University of Tokyo, Tokyo, Japan

(Manuscript received 12 March 2009, in final form 15 July 2009)

Abstract

An improved Mellor–Yamada (MY) turbulence closure model (MYNN model: Mellor–Yamada–Nakanishi–Niino model) that we have developed is summarized and its performance is demonstrated against a large-eddy simulation (LES) of a convective boundary layer. Unlike the original MY model, the MYNN model considers effects of buoyancy on pressure covariances and effects of stability on the turbulent length scale, with model constants determined from a LES database. One-dimensional simulations of Day 33 of the Wangara field experiment, which was conducted in a flat area of southeastern Australia in 1967, are made by the MY and MYNN models and the results are compared with horizontal-average statistics obtained from a three-dimensional LES. The MYNN model improves several weak points of the MY model such as an insufficient growth of the convective boundary layer, and underestimates of the turbulent kinetic energy and the turbulent length scale; it reproduces fairly well the results of the LES including the vertical distributions of the mean and turbulent quantities. The improved performance of the MYNN model relies mainly on the new formulation of the turbulent length scale that realistically increases with decreasing stability, and partly on the parameterization of the pressure covariances and the expression for stability functions for third-order turbulent fluxes.

1. Introduction

Turbulent motions in the atmospheric boundary layer (ABL) are important because they vertically transport sensible and latent heats, which amount to about 60% of the solar radiation absorbed by the earth's surface (Kiehl and Trenberth 1997), thus determining the environment in which the majority of activities of natural beings take place. They also affect the formation of boundary layer clouds that significantly contribute to radiation budgets over polar regions and the Eastern Pacific. Furthermore, turbulent convection in the ABL occasionally triggers cumulus convection, which transports heat and moisture throughout the troposphere, thus affecting the basic structure of the atmosphere.

To express such important roles of turbulent motions in ensemble-mean numerical models, turbulence closure models of several orders have been developed. First-order turbulence closure models, such as the K-profile model (e.g., Troen and Mahrt 1986; Hong et al. 2006), the KE (so-called one-and-a-half order closure) model (e.g., Therry and Lacarrère 1983; Bougeault and Lacarrère 1989), and the standard $k-\varepsilon$ model (e.g., Hanjalic and Launder 1972), have succeeded in reproducing various flow

Corresponding author: Mikio Nakanishi, Department of Earth and Ocean Sciences, National Defense Academy, Yokosuka, Kanagawa 239-8686, Japan.
E-mail: naka@nda.ac.jp

fields. The major weakness of these models, however, is that they need somewhat empirical formulations (e.g., Deardorff 1972) in order to express a countergradient diffusion process resulting from non-local transport, since they relate second-order moments to local gradients of the mean fields through eddy diffusivities. On the other hand, higher-order turbulence closure models can express the countergradient diffusion by predicting second-order moments. Among them, third-order turbulence closure models such as André et al. (1978) and Cheng et al. (2005) have been often used to evaluate lower-order turbulence closure models (e.g., Therry and Lacarrère 1983). The third-order turbulence closure models, however, have a large number of prognostic equations and require large computer resources. They also require many model constants which may not be determined uniquely with confidence.

Second-order turbulence closure models have a less number of prognostic equations than that in the third-order models. A second-order turbulence closure model which is most widely used in a variety of numerical models for geophysical flows is the Mellor–Yamada (MY) model (Mellor and Yamada 1974, 1982). The primary reason for its popularity is that a systematic simplification of the model can be attained according to the degree of anisotropy (Mellor and Yamada 1974) and a relatively simple level-2.5 model having only one prognostic equation for the turbulent kinetic energy (TKE) gives a reasonable prediction (Yamada 1977). Another important reason is that it contains a minimal number of constants which are solely determined from laboratory measurements for neutrally stratified flows and yet predicts reasonably well the observed dimensionless gradient functions in the surface layer over a wide range of stability (Mellor 1973).

Several problems in the MY model, such as a slow growth of a convective boundary layer (e.g., Sun and Ogura 1980) and a rapid decay of turbulence in a stably-stratified nocturnal boundary layer (e.g., Turton and Brown 1987), have been reported, however. Mellor (1973) parameterized higher-order moments such as return-to-isotropy terms without considering buoyancy effects. However, later studies have pointed out that buoyancy effects need to be considered when these terms are parameterized (e.g., Moeng and Wyngaard 1989). Mellor (1973) also assumed that a dominant length scale in the surface layer is given by kz regardless of stability, where k is the von Kármán constant and z is the height. Field observations have shown, however, that the length scale can vary with stability (e.g., Busch and Larsen 1972).

Although most of the previous efforts to improve the MY model focused on excluding singular solutions (e.g., Mellor and Yamada 1982; Galperin et al. 1988; Helfand and Labraga 1988; Gerrity et al. 1994; Janjić 2002), several authors did attempt to improve the problems described above (e.g., Gambo 1978; Sun and Ogura 1980; Kantha and Clayson 1994; Cheng et al. 2002). Using a database of a large-eddy simulation (LES) for dry ABLs under different stratifications, Nakanishi (2001, hereafter N01) recently proposed an improved MY model in which a newly-proposed diagnostic equation for the turbulent length scale and reevaluated model constants are incorporated. Nakanishi and Niino (2004, hereafter NN04) later introduced a partial condensation scheme (Sommeria and Deardorff 1977; Mellor 1977) into the improved MY model, and proposed a convenient computational scheme for its level-3 model. They also used a one-dimensional version of the improved MY model to simulate a radiation fog, and showed that the improved MY model has a good performance comparable to a moist LES model of Nakanishi (2000). Nakanishi and Niino (2006, hereafter NN06) analyzed the singularity and realizability of the improved MY level-3 model, and increased its numerical stability by imposing some restrictions on a time scale L/q and scalar variances, where L is the turbulent length scale and $q^2/2$ the TKE per unit mass. They further incorporated the improved MY model into a three-dimensional regional model, and showed that it predicts a realistic distribution of an advection fog. The improved MY model has been incorporated into an operational nonhydrostatic meso-scale weather prediction model (MSM) at the Japan Meteorological Agency since May 2007 (Hara 2007; Saito et al. 2007), a general circulation model (MIROC: Model for Interdisciplinary Research On Climate) at the Frontier Research Center for Global Change (Chikira and Mochizuki 2007), and an American community meso-scale model (WRF model: Weather Research and Forecasting model), and has been shown to give a good performance. We will hereafter call the improved MY model the MYNN (Mellor–Yamada–Nakanishi–Niino) model to distinguish it from the original MY model.

The first aim of the present paper is to summa-

rize the principal features of the MYNN model that we have developed for the last several years. The second aim is to demonstrate its good performance in a convective mixed layer that develops much deeper ($> 1{,}000$ m) than the convective ABLs of the LES database (N01), which was used to tune the model constants. Day 33 of the Wangara experiment (Clarke et al. 1971) is selected as the target of the present simulation. Since numerous models have simulated this experiment, comparisons with their results would be illuminating. In Section 2 the MYNN model developed by N01, NN04, and NN06 is summarized. In Section 3 several constants in the MYNN model are reevaluated by referring to several recent studies on turbulence closure models. Section 4 compares the results of the MYNN and MY models with those of a LES, and demonstrates the good performance of the MYNN model. Section 5 gives a summary and a discussion on future subjects for the MYNN model.

2. Description of the MYNN model

In the MYNN model, the liquid water potential temperature θ_l ($\equiv \theta - (\theta/T)(L_v/c_p)q_l$) and total water content q_w ($\equiv q_v + q_l$) are used as thermodynamic variables, where θ is the potential temperature, T the absolute temperature, L_v the latent heat of vaporization, c_p the specific heat of dry air at constant pressure, q_l the liquid water content, and q_v the specific humidity.

Notations in the present paper are the same as those in N01, NN04, and NN06; capital letters denote ensemble-averaged variables, small letters turbulent variables, the angle brackets $\langle\ \rangle$ an ensemble average, and the subscript 0 a reference state.

2.1 Equations for mean quantities

The one-dimensional equations for the ensemble-averaged quantities are given by

$$\frac{\partial U}{\partial t} = -\frac{\partial}{\partial z}\langle uw\rangle + f(V - V_g), \tag{1}$$

$$\frac{\partial V}{\partial t} = -\frac{\partial}{\partial z}\langle vw\rangle - f(U - U_g), \tag{2}$$

$$\frac{\partial \Theta_l}{\partial t} = -\frac{\partial}{\partial z}\langle w\theta_l\rangle + \frac{f\Theta_0}{g}\left(V\frac{\partial U_g}{\partial z} - U\frac{\partial V_g}{\partial z}\right), \tag{3}$$

$$\frac{\partial Q_w}{\partial t} = -\frac{\partial}{\partial z}\langle wq_w\rangle, \tag{4}$$

where (u, v, w) are the velocity components, (U_g, V_g) the velocity components of the geostrophic wind, f the Coriolis parameter, and g the gravitational acceleration. The second term on the right-hand side of Eq. (3) represents the horizontal advection of Θ_l obtained from the thermal wind relations.

2.2 Equations for turbulent quantities

To determine the unknown second-order turbulent fluxes such as $\langle uw\rangle$ and $\langle w\theta_l\rangle$, the MYNN model solves equations for second-order turbulent quantities. The one-dimensional equations for these quantities are given by

$$\frac{\partial q^2}{\partial t} = -\frac{\partial}{\partial z}\langle w(u^2 + v^2 + w^2 + 2p/\rho_0)\rangle - 2\left(\langle uw\rangle\frac{\partial U}{\partial z} + \langle vw\rangle\frac{\partial V}{\partial z}\right) + 2\frac{g}{\Theta_0}\langle w\theta_V\rangle - 2\varepsilon, \tag{5}$$

$$\frac{\partial\langle\theta_l^2\rangle}{\partial t} = -\frac{\partial}{\partial z}\langle w\theta_l^2\rangle - 2\langle w\theta_l\rangle\frac{\partial\Theta_l}{\partial z} - 2\varepsilon_{\theta l}, \tag{6}$$

$$\frac{\partial\langle\theta_l q_w\rangle}{\partial t} = -\frac{\partial}{\partial z}\langle w\theta_l q_w\rangle - \langle wq_w\rangle\frac{\partial\Theta_l}{\partial z} - \langle w\theta_l\rangle\frac{\partial Q_w}{\partial z} - 2\varepsilon_{\theta q}, \tag{7}$$

$$\frac{\partial\langle q_w^2\rangle}{\partial t} = -\frac{\partial}{\partial z}\langle wq_w^2\rangle - 2\langle wq_w\rangle\frac{\partial Q_w}{\partial z} - 2\varepsilon_{qw}, \tag{8}$$

where p is the pressure, ρ the air density, θ_V ($\equiv \theta(1 + 0.61q_v - q_l)$) the virtual potential temperature, and ε, $\varepsilon_{\theta l}$, $\varepsilon_{\theta q}$, and ε_{qw} are the dissipation rates of $q^2/2$, $\langle\theta_l^2\rangle/2$, $\langle\theta_l q_w\rangle/2$, and $\langle q_w^2\rangle/2$, respectively.

On the other hand, the Reynolds stresses and second-order turbulent fluxes are given diagnostically by neglecting the time-tendency, advection, and diffusion terms in the case of models of level 3 or less (Mellor and Yamada 1974, 1982): e.g.,

$$\frac{\partial(\langle w^2\rangle - q^2/3)}{\partial t} = 0 = \frac{2}{3}\left(\langle uw\rangle\frac{\partial U}{\partial z} + \langle vw\rangle\frac{\partial V}{\partial z}\right) + \frac{4}{3}\frac{g}{\Theta_0}\langle w\theta_V\rangle + 2\left\langle\frac{p}{\rho_0}\frac{\partial w}{\partial z}\right\rangle, \tag{9}$$

$$\frac{\partial\langle uw\rangle}{\partial t} = 0 = -\langle w^2\rangle\frac{\partial U}{\partial z} + \frac{g}{\Theta_0}\langle u\theta_V\rangle + \left\langle\frac{p}{\rho_0}\left(\frac{\partial u}{\partial z} + \frac{\partial w}{\partial x}\right)\right\rangle, \tag{10}$$

$$\frac{\partial \langle w\theta_l \rangle}{\partial t} = 0 = -\langle w^2 \rangle \frac{\partial \Theta_l}{\partial z} + \frac{g}{\Theta_0}\langle \theta_l \theta_V \rangle + \left\langle \frac{p}{\rho_0}\frac{\partial \theta_l}{\partial z} \right\rangle, \quad (11)$$

where the dissipation rates of $\langle uw \rangle$ and $\langle w\theta_l \rangle$ are neglected based on the local isotropy assumption. The last term on the right-hand side of these equations is called the pressure covariance.

In a level-2.5 model, q^2 is predicted by Eq. (5), but the time-tendency and diffusion terms of Eqs. (6)–(8) are neglected and therefore $\langle \theta_l^2 \rangle$, $\langle \theta_l q_w \rangle$, and $\langle q_w^2 \rangle$ are given diagnostically. In a level-2 model, q^2 is also given diagnostically (Mellor and Yamada 1974, 1982).

2.3 Parameterizations

Second-order turbulence closure models require us to parameterize (a) the dissipation rates, (b) pressure covariances, and (c) third-order turbulent fluxes. Following Mellor (1973), the dissipation rates ε, $\varepsilon_{\theta l}$, $\varepsilon_{\theta q}$, and ε_{qw} are given by

$$\varepsilon = \frac{q^3}{B_1 L}, \quad (12)$$

$$\varepsilon_{\theta l} = \frac{q}{B_2 L}\langle \theta_l^2 \rangle, \quad (13)$$

$$\varepsilon_{\theta q} = \frac{q}{B_2 L}\langle \theta_l q_w \rangle, \quad (14)$$

$$\varepsilon_{qw} = \frac{q}{B_2 L}\langle q_w^2 \rangle, \quad (15)$$

where B_1 and B_2 are closure constants.

The parameterization of the pressure covariances is revised from Mellor (1973), since one of the problems in the MY model is the neglect of buoyancy effects on the pressure covariances (e.g., Moeng and Wyngaard 1989). N01 parameterizes them as

$$\left\langle \frac{p}{\rho_0}\left(\frac{\partial u_i}{\partial x_j} + \frac{\partial u_j}{\partial x_i}\right)\right\rangle = -\frac{q}{3A_1 L}\left(\langle u_i u_j \rangle - \frac{1}{3}q^2\delta_{ij}\right) + C_1 q^2\left(\frac{\partial U_i}{\partial x_j} + \frac{\partial U_j}{\partial x_i}\right) - C_2\frac{g}{\Theta_0}\left(\langle u_i\theta_V\rangle\delta_{j3} + \langle u_j\theta_V\rangle\delta_{i3} - \frac{2}{3}\langle u_3\theta_V\rangle\delta_{ij}\right) + C_4\left(\langle u_i u_k\rangle\frac{\partial U_j}{\partial x_k} + \langle u_j u_k\rangle\frac{\partial U_i}{\partial x_k} - \frac{2}{3}\langle u_k u_l\rangle\frac{\partial U_k}{\partial x_l}\delta_{ij}\right), \quad (16)$$

$$\left\langle \frac{p}{\rho_0}\frac{\partial \theta_l}{\partial x_i}\right\rangle = -\frac{q}{3A_2 L}\langle u_i\theta_l\rangle - C_3\frac{g}{\Theta_0}\langle \theta_l\theta_V\rangle\delta_{i3} + C_5\langle u_k\theta_l\rangle\frac{\partial U_i}{\partial x_k}, \quad (17)$$

where $(u_1, u_2, u_3) = (u, v, w)$ are the velocity components in the directions of $(x_1, x_2, x_3) = (x, y, z)$, respectively, δ_{ij} the Kronecker's delta, and A_1, A_2, and C_1–C_5 closure constants. The terms with A_1 and A_2 represent the return-to-isotropy hypothesis of Rotta, while the terms with C_1, C_4, and C_5 and those with C_2 and C_3 represent effects of shear and buoyancy, respectively. This parameterization is more elaborate than that by Mellor (1973) who neglected the terms with C_2–C_5, but is slightly simpler than that by Sun and Ogura (1980) or Cheng et al. (2002). We will eliminate the term with C_4 by setting $C_4 = 0$ because, for unstable conditions, this term tends to predict $\langle u^2 \rangle$ smaller than our LES data (N01). The values of the other closure constants will be given in Section 3.

The parameterization of the third-order turbulent fluxes will be described in the following subsection.

2.4 Turbulent fluxes

Through the diagnostic equations such as Eqs. (9)–(11) and the parameterization of the pressure covariances, models of level 3 or less can express the second-order turbulent fluxes in the form of gradient diffusion (N01; NN04; NN06):

$$-\langle uw \rangle = LqS_M\frac{\partial U}{\partial z}, \quad (18)$$

$$-\langle vw \rangle = LqS_M\frac{\partial V}{\partial z}, \quad (19)$$

$$-\langle w\theta_l \rangle = LqS_H\frac{\partial \Theta_l}{\partial z} = Lq\left(S_{H2.5}\frac{\partial \Theta_l}{\partial z} + \Gamma_\theta\right), \quad (20)$$

$$-\langle wq_w \rangle = LqS_H\frac{\partial Q_w}{\partial z} = Lq\left(S_{H2.5}\frac{\partial Q_w}{\partial z} + \Gamma_q\right), \quad (21)$$

$$-\langle w\theta_V \rangle = -\beta_\theta\langle w\theta_l\rangle - \beta_q\langle wq_w\rangle, \quad (22)$$

where S_M ($\equiv S_{M2.5} + S'_M$) and S_H ($\equiv S_{H2.5} + S'_H$) are stability functions for a level-3 model for momentum, and heat and moisture, respectively, the subscript 2.5 denotes a level-2.5 model, the prime difference between the level-3 and level-2.5 models. Γ_θ ($\equiv S'_H \partial\Theta_l/\partial z$) and Γ_q ($\equiv S'_H \partial Q_w/\partial z$) are functions that represent effects of countergradient diffusion, as will be shown in the following subsection. β_θ and β_q are functions determined from the condensation process, which are described in Appendix B.

The third-order turbulent fluxes need to be parameterized. NN04 adopts expressions similar to the gradient diffusion of the MY model as

$$-\langle w(u^2 + v^2 + w^2 + 2p/\rho_0)\rangle = LqS_q \frac{\partial q^2}{\partial z}, \quad (23)$$

$$-\langle w\theta_l^2\rangle = LqS_{\theta l} \frac{\partial\langle\theta_l^2\rangle}{\partial z}, \quad (24)$$

$$-\langle w\theta_l q_w\rangle = LqS_{\theta q} \frac{\partial\langle\theta_l q_w\rangle}{\partial z}, \quad (25)$$

$$-\langle wq_w^2\rangle = LqS_{qw} \frac{\partial\langle q_w^2\rangle}{\partial z}, \quad (26)$$

where S_q, $S_{\theta l}$, $S_{\theta q}$, and S_{qw} are also stability functions.

2.5 Stability functions

N01, NN04, and NN06 decomposed the stability functions S_M and S_H into two parts: The first part is given by the corresponding stability functions $S_{M2.5}$ and $S_{H2.5}$ for the level-2.5 model, and the second part their corrections S'_M and S'_H. After considerable algebra, they are obtained as

$$S_{M2.5} = \alpha_c A_1 \frac{\Phi_3 - 3C_1\Phi_4}{D_{2.5}}, \quad (27)$$

$$S_{H2.5} = \alpha_c A_2 \frac{\Phi_2 + 3C_1\Phi_5}{D_{2.5}}, \quad (28)$$

$$S'_M = \alpha_c A_1 \frac{\Phi_3 - \Phi_4}{D'}\Phi', \quad (29)$$

$$S'_H = \alpha_c A_2 \frac{\Phi_2 + \Phi_5}{D'}\Phi', \quad (30)$$

where notations follow NN06,

$$D_{2.5} = \Phi_2\Phi_4 + \Phi_5\Phi_3, \quad (31)$$

$$D' = \Phi_2(\Phi_4 - \Phi_1 + 1) + \Phi_5(\Phi_3 - \Phi_1 + 1), \quad (32)$$

$$\Phi_1 = 1 - 3\alpha_c^2 A_2 B_2 (1 - C_3) G_H, \quad (33)$$

$$\Phi_2 = 1 - 9\alpha_c^2 A_1 A_2 (1 - C_2) G_H, \quad (34)$$

$$\Phi_3 = \Phi_1 + 9\alpha_c^2 A_2^2 (1 - C_2)(1 - C_5) G_H, \quad (35)$$

$$\Phi_4 = \Phi_1 - 12\alpha_c^2 A_1 A_2 (1 - C_2) G_H, \quad (36)$$

$$\Phi_5 = 6\alpha_c^2 A_1^2 G_M, \quad (37)$$

$$\Phi' = 3(1 - C_3) G_H (C_\theta - \alpha_c B_2 S_{H2.5}), \quad (38)$$

$$G_M = \frac{L^2}{q^2}\left[\left(\frac{\partial U}{\partial z}\right)^2 + \left(\frac{\partial V}{\partial z}\right)^2\right], \quad (39)$$

$$G_H = -\frac{L^2}{q^2}\frac{g}{\Theta_0}\left(\beta_\theta \frac{\partial\Theta_l}{\partial z} + \beta_q \frac{\partial Q_w}{\partial z}\right) \equiv -\frac{L^2}{q^2}\frac{g}{\Theta_0}\frac{\partial\Theta_V}{\partial z}, \quad (40)$$

$$C_\theta = \frac{\langle\theta_l^2\rangle}{L^2(\partial\Theta_l/\partial z)^2} = \frac{\langle\theta_l q_w\rangle}{L^2(\partial\Theta_l/\partial z)(\partial Q_w/\partial z)}, \quad (41)$$

$$\alpha_c \equiv 1 - \alpha = \begin{cases} q/q_2, & q < q_2 \\ 1, & q \geq q_2, \end{cases} \quad (42)$$

and α is a function introduced by Helfand and Labraga (1988) to ensure nonsingular solutions for growing turbulence. $q_2^2/2$ is the TKE per unit mass given by the level-2 model (Appendix A).

When $\partial\Theta_l/\partial z$ and $\partial Q_w/\partial z$ are small, C_θ in Eq. (41) diverges. To avoid this problem, the functions S'_M, $S'_H G_H$, Γ_θ, and Γ_q are computed as

$$S'_M = E_M\left(\frac{L}{q^2}\frac{g}{\Theta_0}\right)^2(\langle\theta_V^2\rangle - \langle\theta_V^2\rangle_{2.5}), \quad (43)$$

$$S'_H G_H = E_H\left(\frac{L}{q^2}\frac{g}{\Theta_0}\right)^2(\langle\theta_V^2\rangle - \langle\theta_V^2\rangle_{2.5}), \quad (44)$$

$$\Gamma_\theta = -E_H\frac{1}{q^2}\frac{g}{\Theta_0}(\langle\theta_l\theta_V\rangle - \langle\theta_l\theta_V\rangle_{2.5}), \quad (45)$$

$$\Gamma_q = -E_H\frac{1}{q^2}\frac{g}{\Theta_0}(\langle q_w\theta_V\rangle - \langle q_w\theta_V\rangle_{2.5}), \quad (46)$$

where

$$E_M = 3\alpha_c A_1 (1 - C_3)\frac{\Phi_3 - \Phi_4}{D' G_H}, \quad (47)$$

$$E_H = 3\alpha_c A_2 (1 - C_3)\frac{\Phi_2 + \Phi_5}{D'}, \quad (48)$$

$$\langle\theta_l\theta_V\rangle = \beta_\theta\langle\theta_l^2\rangle + \beta_q\langle\theta_l q_w\rangle, \quad (49)$$

$$\langle q_w\theta_V\rangle = \beta_\theta\langle\theta_l q_w\rangle + \beta_q\langle q_w^2\rangle, \quad (50)$$

$$\langle\theta_V^2\rangle = \beta_\theta\langle\theta_l\theta_V\rangle + \beta_q\langle q_w\theta_V\rangle. \quad (51)$$

Note that the sign of E_H in this paper is taken to be opposite to that in NN04.

Although $S_{M2.5}$ and $S_{H2.5}$ are always nonnegative (Helfand and Labraga 1988), S'_M can become negative and S'_H can approach even negative infinity (Eqs. 43 and 44). This means that the level-3 model is capable of expressing the countergradient diffusion as shown by Γ_θ and Γ_q (Eqs. 45 and 46) with the help of the prognostic equations of Eqs. (6)–(8).

As to the stability functions S_q, $S_{\theta l}$, $S_{\theta q}$, and S_{qw}, Mellor and Yamada (1982) set all of them to a constant value of 0.2. Based on our LES database (N01), however, we assume them to be proportional to S_M; their proportionality constants will be shown in Section 3.

2.6 Equations for the turbulent length scale

One of the problems in the MY model is that there exists no reliable expression for the turbulent length scale L. Based on the LES database, N01 proposed a new diagnostic equation for L, which is designed to be controlled by the smallest length scale among the three length scales L_S, L_T, and L_B:

$$\frac{1}{L}=\frac{1}{L_S}+\frac{1}{L_T}+\frac{1}{L_B}, \tag{52}$$

$$L_S=\begin{cases} kz/3.7, & \zeta \geq 1 \\ kz(1+2.7\zeta)^{-1}, & 0 \leq \zeta < 1 \\ kz(1-100\zeta)^{0.2}, & \zeta < 0, \end{cases} \tag{53}$$

$$L_T=0.23\frac{\int_0^\infty qz\,dz}{\int_0^\infty q\,dz}, \tag{54}$$

$$L_B=\begin{cases} q/N, & \partial\Theta_V/\partial z>0 \text{ and } \zeta \geq 0 \\ [1+5(q_c/L_TN)^{1/2}]q/N, & \partial\Theta_V/\partial z>0 \text{ and } \zeta<0 \\ \infty, & \partial\Theta_V/\partial z \leq 0, \end{cases} \tag{55}$$

where ζ ($\equiv z/L_M$) is the dimensionless height, L_M ($\equiv -\Theta_0 u_*^3/kg\langle w\theta_V\rangle_g$) the Monin–Obukhov length, u_* the friction velocity, N ($\equiv [(g/\Theta_0)\partial\Theta_V/\partial z]^{1/2}$) the Brunt–Väisälä frequency, and the subscript g denotes the ground surface. q_c ($\equiv [(g/\Theta_0)\langle w\theta_V\rangle_g L_T]^{1/3}$) is a velocity scale defined similarly as the convective velocity w_*, except that the depth z_i of the convective ABL is replaced by L_T.

L_S is the length scale in the surface layer, which increases with height and is effective to L only near the surface. L_T is the length scale dependent on the depth of the ABL (Mellor and Yamada 1974) and is independent of height. L_B is related to the buoyancy length scale q/N, which characterizes the distance to which an air parcel having TKE of $q^2/2$ can move vertically against the buoyancy force; it is therefore effective only in a stable layer. The empirical constants that appear in Eqs. (53)–(55) were determined from the LES database (N01).

We will now describe how we have selected the functional forms given by Eqs. (53) and (55). Note that the expression for L_T (Eq. 54) follows Mellor and Yamada (1974) except for the proportionality constant. L_S for $\zeta \geq 0$ is given by the best fit curve for the dissipation length scale L_ε in the surface layer estimated from the LES data. For $\zeta<0$, the best fit curve for L_ε in the surface layer was subject to height, but that for L_ε at the same height seemed to have a functional form of $(-\zeta)^{0.2}$. The constant value of 100 in Eq. (53) was then determined in order that L fits L_ε from the LES data.

When L_B for $\partial\Theta_V/\partial z>0$ is given by q/N, it is likely that the length scale in the upper half of the convective ABL is underestimated, because TKE there would be increased through the turbulent transport and buoyancy production. According to Moeng and Sullivan (1994), the rate of this increase of TKE in the highly convective ABL is nearly proportional to w_*^3/z_i. N01 assumed that, in the upper part of the ABL, the time scale is given by N^{-1} and the rate of the increase of TKE, $w_*^3/z_i=w_*^2 w_*/z_i$, may be replaced by q^2q_c/L_T. This replacement is made because q^2q_c/L_T can vanish above the ABL and L_T has a characteristic similar to z_i. The addition of the square root of q^2q_c/L_TN to q leads to the expression in Eq. (55)[1].

2.7 Nonsingular and realizable level-3 model

NN04 proposed a new scheme to stably integrate the level-3 model. NN06 later analyzed the singularity and realizability of the level-3 model and simplified the scheme. NN06 showed that nonsingular solutions of S'_M and S'_H can be attained by ensuring $\Phi_3-\Phi_1+1>0$ ($D'>0$) in Eq. (32) under stable stratification and imposing a restriction on a time scale L/q such that

$$\frac{L}{q} \leq \frac{1}{N} \quad \text{for } \frac{\partial\Theta_V}{\partial z}>0, \tag{56}$$

1 The square root should have been computed after the addition of q^2q_c/L_TN to q^2. In that case an optimal value of the empirical constant in Eq. (55) is 40 instead of 5: i.e., $(1+40q_c/L_TN)^{1/2}q/N$. This modification, however, has little effect on simulated results.

when Eqs. (43)–(46) are computed. This restriction becomes substantial in the upper part of the convective ABL.

On the other hand, Rotta's hypothesis requires a restriction on the normalized velocity variances $C_u \equiv \langle u^2 \rangle / q^2$, $C_v \equiv \langle v^2 \rangle / q^2$, and $C_w \equiv \langle w^2 \rangle / q^2$ (e.g., Mellor and Yamada 1982). NN06 similarly imposed restrictions of $C_u \geq 0.12$, $C_v \geq 0.12$, and $C_w \geq 0.12$. We here simply impose a restriction on C_w as

$$0.12 \leq C_w \leq 0.76, \tag{57}$$

which means that $C_w \geq 0.12$ and $C_u + C_v \geq 0.24$ are assured, but that $C_u \geq 0.12$ and $C_v \geq 0.12$ are not necessarily so. Normalization of Eq. (9) with our parameterizations gives

$$C_w = C_{w2.5} + E_w \left(\frac{L}{q^2} \frac{g}{\Theta_0} \right)^2 (\langle \theta_V^2 \rangle - \langle \theta_V^2 \rangle_{2.5}), \tag{58}$$

where

$$C_{w2.5} = \frac{\Phi_1}{3} \frac{\Phi_2 + 3C_1\Phi_5}{D_{2.5}}, \tag{59}$$

$$E_w = (1 - C_3) \frac{\Phi_2(\Phi_1 - \Phi_4) + \Phi_5(\Phi_1 - \Phi_3)}{D' G_H}. \tag{60}$$

The restriction on C_w (Eq. 57) therefore results in that on $\langle \theta_V^2 \rangle$:

$$\begin{aligned} 0.12 - C_{w2.5} &\leq E_w \left(\frac{L}{q^2} \frac{g}{\Theta_0} \right)^2 (\langle \theta_V^2 \rangle - \langle \theta_V^2 \rangle_{2.5}) \\ &\leq 0.76 - C_{w2.5}. \end{aligned} \tag{61}$$

Although this restriction is imposed only on $\langle \theta_V^2 \rangle$, it affects the production of TKE (Eq. $43 \times G_M$ and Eq. 44) and may also control the other scalar variances indirectly.

Note that these restrictions are imposed to obtain realistic solutions of Eqs. (43)–(46), but not necessarily to assure nonnegative S_M $(= S_{M2.5} + S'_M)$ for numerical stability of the level-3 model (Eqs. 1, 2, 18, and 19).

3. Closure constants in the MYNN model

By referring to several recent studies on turbulence closure models, we will reexamine the closure constants and also the proportionality constants in the stability functions for the third-order turbulent fluxes.

N01 estimated a set of the closure constants from the LES data as

$$\begin{aligned} &(A_1, A_2, B_1, B_2, C_1) \\ &\quad = (1.18, 0.665, 24.0, 15.0, 0.137), \\ &(C_2, C_3, C_4, C_5) = (0.65, 0.294, 0.0, 0.2), \end{aligned} \tag{62}$$

where

$$A_1 = B_1 \frac{1 - 3\gamma_1}{6}, \tag{63}$$

$$A_2 = \frac{1}{3\gamma_1 B_1^{1/3}}, \tag{64}$$

$$C_1 = \gamma_1 - \frac{1}{3A_1 B_1^{1/3}}, \tag{65}$$

$\gamma_1 = 0.235$, and $\mathrm{Pr} = 0.74$. However, the value of C_3 in Eq. (62) is out of the range between the theoretical value of 1/3 for isotropic turbulence (e.g., Gibson and Launder 1978) and a suggested value of 1/2 for a convective ABL (Moeng and Wyngaard 1986). N01, after determining the other closure constants, chose the value of C_3 in order that the slope of the dimensionless gradient function ϕ_h for heat approaches 4.7 as $\zeta \to \infty$ (Businger et al. 1971), where C_2 was selected to be 0.65 following Gambo (1978). If C_2 is selected to be 0.75, however, C_3 becomes 0.352 and falls within the range of the previous studies. These revised values of C_2 and C_3 reduce the magnitude of S_M in the convective ABL and lead to a better agreement of S_M from the MYNN model with that from the LES data (Fig. 1). Furthermore, the MYNN model with these values of C_2 and C_3 increases the critical gradient Richardson number Ri_c to 0.95 (Appendix A), which is very close to $\mathrm{Ri}_c \sim 1$ as suggested by laboratory data, numerical simulations, and a nonlinear analysis (cf., Cheng et al. 2002, 2003). Thus we have a new set of the closure constants as

$$\begin{aligned} &(A_1, A_2, B_1, B_2, C_1) \\ &\quad = (1.18, 0.665, 24.0, 15.0, 0.137), \\ &(C_2, C_3, C_4, C_5) \\ &\quad = (0.75, 0.352, 0.0, 0.2). \end{aligned} \tag{66}$$

Figure 2 shows the dependence of the stability functions S_{M2} and S_{H2} on Ri for the level-2 models (Appendix A) of the MYNN model with Eq. (66) and the MY model with closure constants of Mellor and Yamada (1982). For positive (negative) Ri, S_{M2} and S_{H2} in the MYNN model are larger

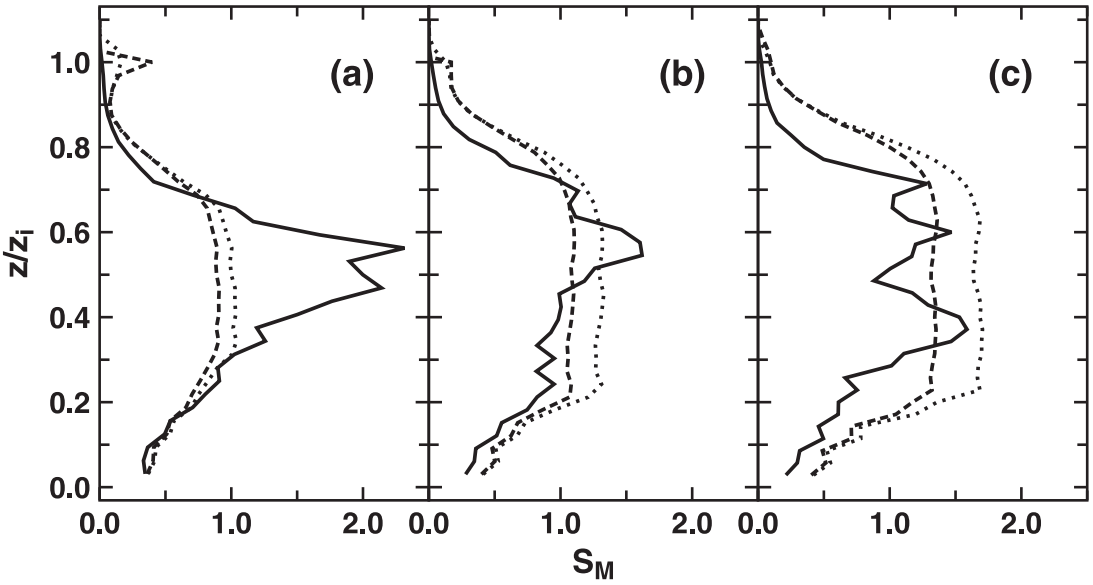

Fig. 1. Comparisons of the stability function S_M obtained from the MYNN level-3 model with Eqs. (62) (dotted line) and (66) (dashed line) with that from the LES (solid line) for convective ABLs. The ratios of the ABL depth z_i to the Monin–Obukhov length L_M are (a) −4, (b) −11, and (c) −24. S_M from the LES fluctuates, because it is computed using the vertical shear which is small in the convective ABL (Adapted from Nakanishi 2001).

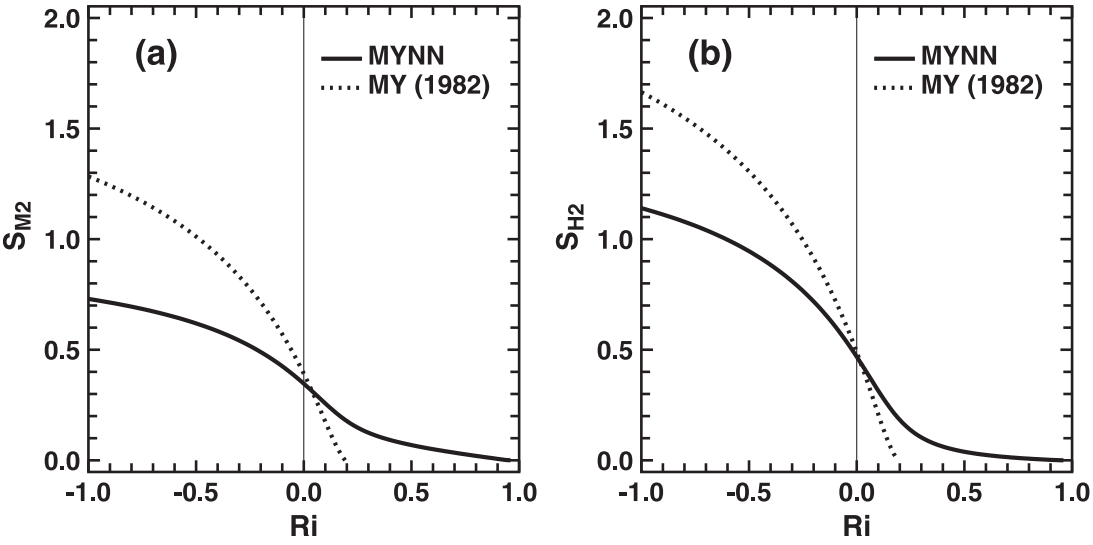

Fig. 2. Stability functions, S_{M2} and S_{H2}, for the level-2 model as a function of the gradient Richardson number Ri. MYNN (solid line) and MY (dotted line) represent the MYNN and MY models, respectively.

(smaller) than those in the MY model. The larger magnitudes of S_{M2} and S_{H2} in the MYNN model for positive Ri may solve the problem of a rapid decay of turbulence in a stable ABL (e.g., Turton and Brown 1987).

It is often claimed that the downgradient-diffusion formulation of the third-order turbulent fluxes (Eqs. 23–26) is inadequate in the convective ABL (e.g., Moeng and Wyngaard 1989). Results of N01 have shown, however, that this formulation

gives a relatively good approximation at least to our LES data, and that the stability functions S_q and $S_{\theta l}$ are likely to be well represented by functions of S_M. NN04 then assumed the stability functions S_q, $S_{\theta l}$, $S_{\theta q}$, and S_{qw} to be proportional to S_M, and set all the proportionality constants to 2, for simplicity (e.g., Deardorff 1980). More detailed observations of the figures of N01 reveal that S_q is several times larger than S_M, while $S_{\theta l}$ is nearly equal to S_M. To obtain a better performance, we will revise the proportionality as

$$S_q = 3S_M, \tag{67}$$

$$S_{\theta l} = S_{\theta q} = S_{qw} = S_M. \tag{68}$$

Although the present parameterization of the third-order turbulent fluxes may be less sophisticated in comparison with the one that incorporates the production of their fluxes due to buoyancy (e.g., Therry and Lacarrère 1983; Canuto et al. 1994; Abdella and McFarlane 1997), the stability functions in Eqs. (67) and (68) include the buoyancy effects through S_M.

4. Performance of the MYNN model

To demonstrate the performance of the MYNN model, we report the results of one-dimensional simulation of Day 33 of the Wangara experiment (Clarke et al. 1971), which has been often used to verify numerical simulation models. The results together with those of a one-dimensional simulation by the MY model are compared with those of a three-dimensional LES instead of the observational data, because the observed boundary layer is affected by a large-scale subsidence (e.g., Deardorff 1974; Yamada and Mellor 1975) and is not directly compared with the simulated one.

4.1 Outline of one-dimensional simulation

For such a convective ABL on a clear day as observed on Day 33 of the Wangara experiment, the condensation of water vapor needs very little to be considered. Thus the condensation and radiation processes are excluded in the present simulation. The governing equations are the same as described in Section 2, except that q_l is equal to zero and therefore θ_l and q_w are equivalent to θ and q_v, respectively.

The boundary condition at the ground surface is given in the form of the turbulent fluxes. Following Wyngaard and Coté (1974), the heat and moisture fluxes $\langle w\theta_l\rangle_g$ and $\langle wq_w\rangle_g$ at the ground surface are prescribed as functions of time:

$$\langle w\theta_l\rangle_g(t) = 2.16\times10^{-1}\cos\left(\frac{t-13}{11}\pi\right)\ \mathrm{K\ m\ s^{-1}}, \tag{69}$$

$$\langle wq_w\rangle_g(t) = 2.29\times10^{-5}\cos\left(\frac{t-13}{11}\pi\right)\ \mathrm{m\ s^{-1}}, \tag{70}$$

where t is the elapsed time in hours from 0000 LST. The surface momentum flux, on the other hand, is calculated from Monin–Obukhov similarity theory with the dimensionless gradient functions of Businger et al. (1971), where the roughness length is set to 0.01 m.

The top boundary is treated as a stress-free rigid lid:

$$\frac{\partial U}{\partial z} = \frac{\partial V}{\partial z} = \frac{\partial Q_w}{\partial z} = 0, \tag{71}$$

$$\frac{\partial \Theta_l}{\partial z} = 0.0075\ \mathrm{K\ m^{-1}}. \tag{72}$$

Initial conditions for (U, V), Θ_l, and Q_w are given by the observational data at 0900 LST on Day 33 (16 August 1967) of the Wangara experiment (Clarke et al. 1971). The geostrophic wind is assumed to be independent of time (Deardorff 1974); U_g varies linearly from -5.5 m s^{-1} at the surface to -2.6 m s^{-1} at $z = 1$ km, and then to -1.2 m s^{-1} at $z = 2$ km, and V_g is 0 m s^{-1} at all heights.

The vertical computational domain consists of 50 layers with a uniform grid spacing of 40 m. Spatial derivatives are approximated by a centered difference scheme of second-order accuracy. Time integration of the equations is performed until 1600 LST using the Crank–Nicholson scheme with a time step of 2 s. Such a small time step is used in order to assure the same conditions as the LES.

Note that, to obtain nonsingular solutions, a restriction on L/q as in Eq. (56) has to be strengthened to $L/q \le 0.45/N$ for the MY model because of the different closure constants.

4.2 Outline of three-dimensional LES

The LES model used in this study is the same as that of Nakanishi (2000), except that the subgrid turbulent fluxes are determined from the standard Smagorinsky–Lilly model, because the two-part model of Sullivan et al. (1994), which is composed of isotropic and anisotropic parts, is considered to have only a minor effect on a simulation of a convective ABL. The Smagorinsky constant is 0.18.

The turbulent Prandtl number is 1/3 for unstable and neutral conditions, and increases with increasing stability to 1 above the Richardson number of 0.25 (Nakanishi 2000).

The bottom and top boundary conditions are the same as those of the one-dimensional simulations, except for the conditions that the vertical velocity component vanishes at these boundaries and Monin–Obukhov similarity theory is applied to horizontally-averaged quantities. A sponge layer for avoiding reflections of the gravity waves from the top boundary is not placed. The lateral boundaries are periodic.

In the LES, small random perturbations are initially added to all velocity components below a height of 100 m. A "spin-up" process for generating a realistic intensity of turbulence is skipped because turbulence grows quickly without such a process in a convective ABL.

The computational domain of the LES consists of 125×125 grid boxes horizontally and 50 layers vertically. A uniform grid spacing of 40 m is used in all directions. Time integration of the equations is done using the Adams–Bashforth scheme and SMAC method. When solving the Poisson equation for the pressure, Fourier expansion is applied to the horizontal directions. The LES are also run with a time step of 2 s until 1600 LST.

LES has demonstrated the good ability to reproduce turbulence properties in various types of turbulent flows (e.g., Schmidt and Schumann 1989; Andrén 1995). The results of our LES compare well with those of previous LESs of the Wangara experiment (e.g., Deardorff 1974; Golaz et al. 2002).

4.3 Results

The results of the MYNN and MY models are compared with horizontally-averaged total (resolved plus subgrid scales) quantities of the LES, which are considered to approximate the ensemble averages. In expectation of wide applications of the MYNN model, the results of the MYNN level-2.5 model are also shown. Compared with the level-3 model, the level-2.5 model reduces the computational cost of the turbulence process by about 40%, because it does not require the prognostic equations for scalar variances (Eqs. 6–8).

a. Potential temperature

Figure 3 shows vertical profiles of potential temperature at every two hours between 1000 and 1600 LST obtained from the MYNN level-3 (NN30), MY level-3 (MY30), MYNN level-2.5 (NN25) models, and the LES, where the initial profile at 0900 LST is also shown. NN30 shows excellent agreement with the LES results (Fig. 3a); it nicely predicts the growth of the ABL with time, a weakly stable stratification in the upper half of the ABL, and the decrease of potential temperature due to the convection penetrating into the overlying stable

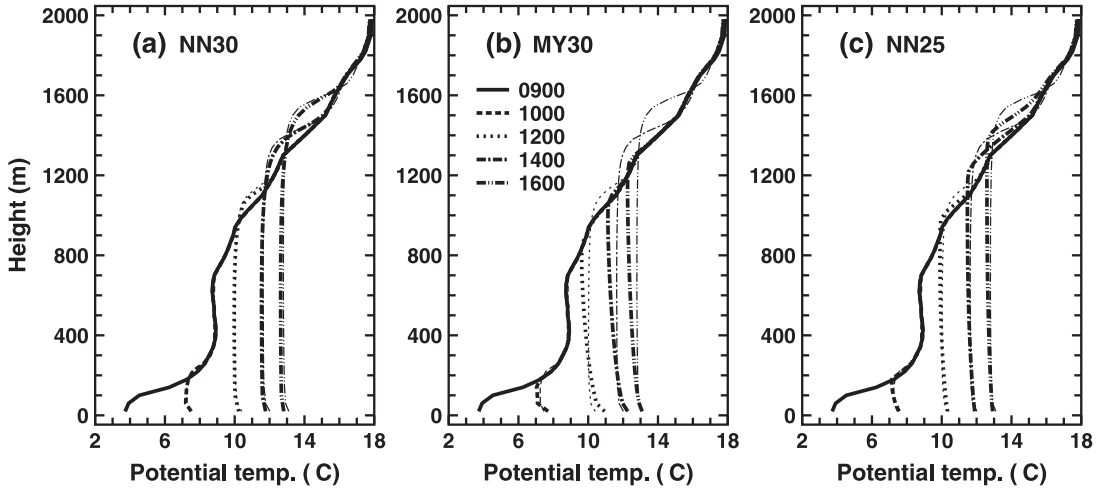

Fig. 3. Vertical profiles of potential temperature obtained from the (a) MYNN level-3 (NN30), (b) MY level-3 (MY30), and (c) MYNN level-2.5 (NN25) models. Thin lines represent the LES results, which are horizontally-averaged total (resolved plus subgrid scales) quantities. Numerals in the legend mean the time in LST.

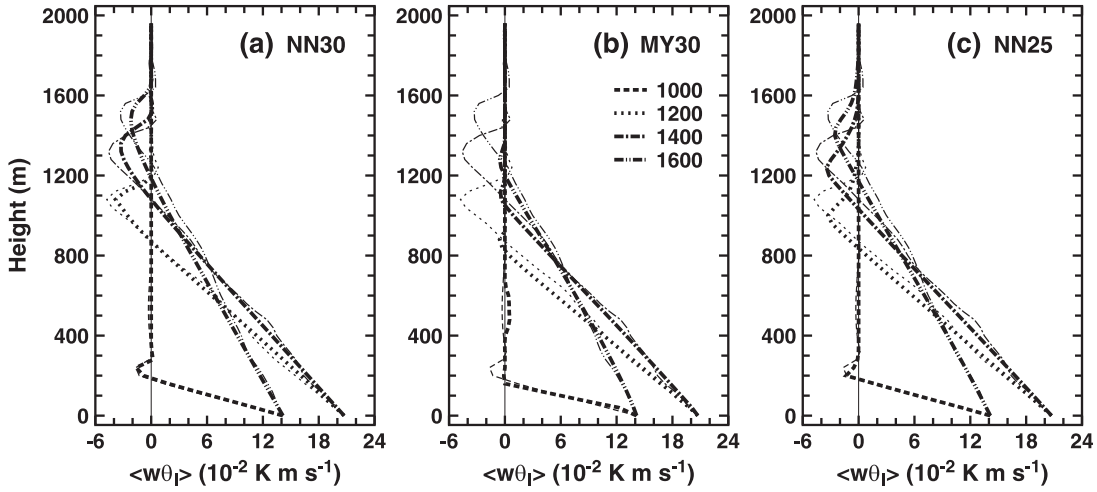

Fig. 4. Same as Fig. 3 but for the vertical heat flux $\langle w\theta_l \rangle$.

layer (the entrainment zone). On the other hand, MY30 reproduces the LES results less satisfactorily (Fig. 3b); the growth of the ABL is insufficient, unstable stratification prevails throughout the ABL, and the entrainment zone is very thin. NN25 also predicts a slightly unstable stratification throughout the ABL (Fig. 3c). With respect to the growth of the ABL and the entrainment zone, however, it gives much better agreement with the LES results than MY30 does.

Figure 4 shows vertical profiles of heat flux. Below the inversion, the heat flux predicted by the three models agrees well with that in the LES. The combination of Figs. 3 and 4 reveals that only NN30 is able to reproduce the countergradient diffusion in the weakly stable layer in the upper half of the ABL. Near the inversion, on the other hand, MY30 considerably underestimates the negative heat flux (Fig. 4b), implying an inability to incorporate the effects of the penetrative convection and entrainment. Although the absolute values of the minimum heat flux in NN30 and NN25 are somewhat smaller than those in the LES (Figs. 4a,c), they are significantly larger than those in MY30 (Fig. 4b).

Parameters of the convective mixed layer as obtained from the different models are summarized in Table 1. The ratio R of the minimum value of the vertical heat flux to its surface value, the depth z_i of the mixed layer, and the convective velocity w_* by NN30 are all predicted more closely to those of the LES than those by MY30. It is also noted that even NN25 gives a better performance than MY30 does. z_i predicted by the LES and NN30 is larger than that of the Wangara observational data. This is considered to be due to a large-scale subsidence, the magnitude of which is unknown and can be only determined so as to better reproduce the ob-

Table 1. Parameters of the convective mixed layer as obtained from the models. NN30, MY30, and NN25 indicate the MYNN level-3, MY level-3, and MYNN level-2.5 models, respectively. R is the ratio of the minimum value of the vertical heat flux to its surface value, z_i the height at which its minimum value occurs, and $w_* = [(g/\Theta_0)\langle w\theta_V \rangle_g z_i]^{1/3}$.

Time	$-R$				z_i (m)				w_* (m s^{-1})			
(LST)	LES	NN30	MY30	NN25	LES	NN30	MY30	NN25	LES	NN30	MY30	NN25
1000	0.117	0.114	0.009	0.095	240	240	200	200	1.06	1.06	1.00	1.00
1200	0.230	0.185	0.027	0.158	1080	1080	880	1000	1.99	1.99	1.86	1.94
1400	0.221	0.157	0.022	0.167	1320	1360	1120	1240	2.13	2.15	2.02	2.09
1600	0.233	0.154	0.039	0.181	1520	1480	1280	1400	1.97	1.95	1.86	1.91

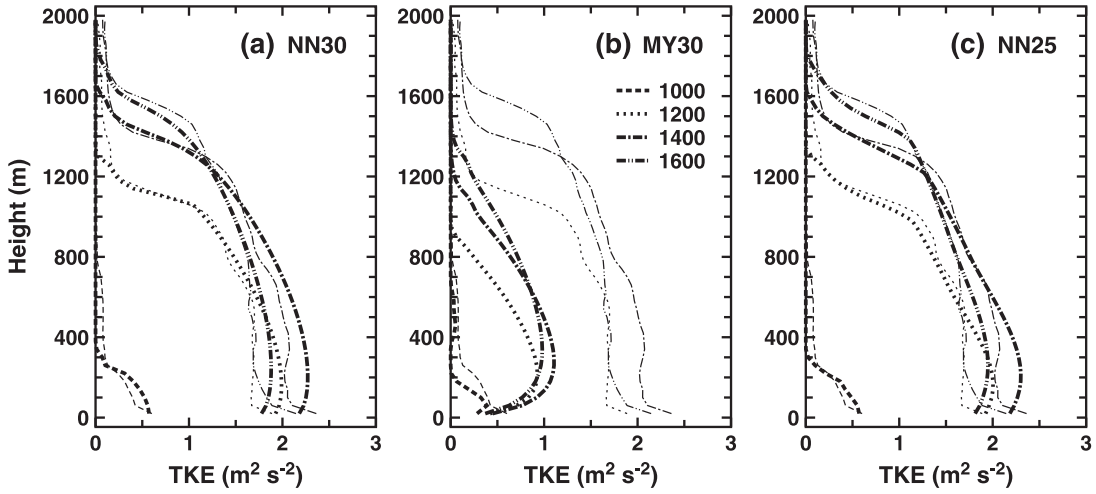

Fig. 5. Same as Fig. 3 but for the TKE.

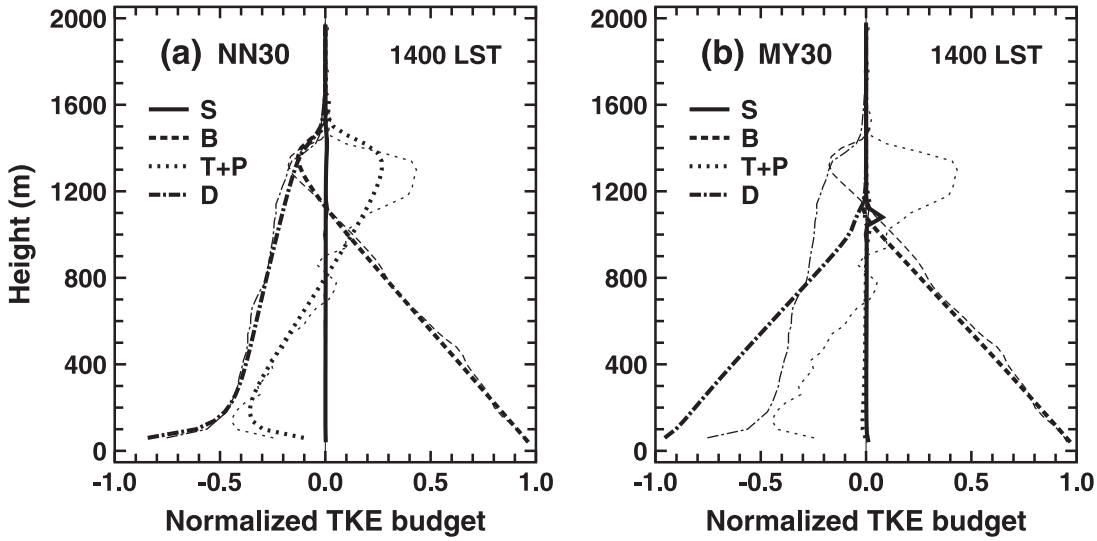

Fig. 6. TKE budget normalized by w_*^3/z_i at 1400 LST, obtained from the (a) MYNN level-3 (NN30) and (b) MY level-3 (MY30) models. Thin lines represent the LES results. S (solid line) means the shear production, B (dashed line) the buoyancy production, T + P (dotted line) the turbulent and pressure transports, and D (dash-dotted line) the dissipation rate.

servational data (e.g., Deardorff 1974; Golaz et al. 2002).

b. TKE

Figure 5 shows vertical profiles of TKE from the three one-dimensional models and the LES. NN30 reproduces the LES results very well except near the surface (Fig. 5a). NN25 also predicts TKE profiles similar to the LES results (Fig. 5c). On the other hand, the magnitude of TKE in MY30 is only a half of that in the LES throughout the ABL (Fig. 5b).

Figure 6 shows the TKE budget normalized by w_*^3/z_i at 1400 LST for NN30 and MY30, where the results of NN25 are omitted because they are fairly similar to those of NN30. NN30 is in excellent agreement with the LES results (Fig. 6a). Since the vertical wind shear is small (not shown), the

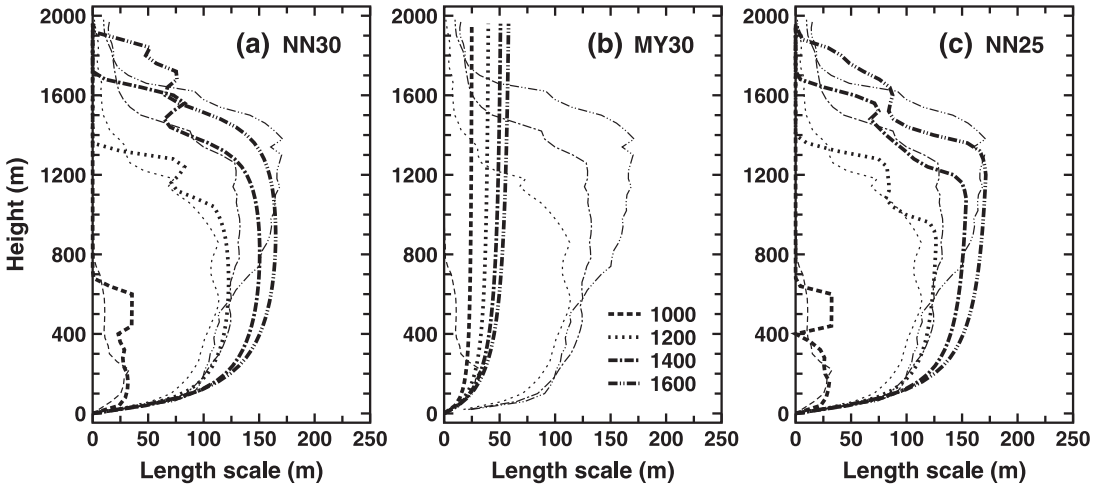

Fig. 7. Same as Fig. 3 but for the turbulent length scale.

shear production S is negligibly small in all models. The sum of the turbulent and pressure transports, T + P, in NN30 and the LES has a large negative (positive) value near the surface (the ABL top), showing that the TKE is transported from the lower part to the upper part of the ABL. However, T + P in MY30 are considerably smaller than that in the LES (Fig. 6b), mainly because the stability function for the third-order turbulent fluxes in MY30 is given by $S_q = 0.2$, which is considerably smaller than Eq. (67). Consequently, the buoyancy production B nearly balances the dissipation rate D in MY30.

c. *Turbulent length scale*

Figure 7 shows vertical profiles of turbulent length scale L from the three one-dimensional models and the LES, where L in MY30 is estimated from the diagnostic equation of Mellor and Yamada (1974) instead of the prognostic equation of Mellor and Yamada (1982), and L in the LES is estimated from the dissipation rate in the TKE equation. The turbulent length scale L in NN30 and NN25 is comparable to or slightly larger than that in the LES (Figs. 7a,c), while L in MY30 is considerably smaller than that in the LES (Fig. 7b). This smaller L in MY30 causes the smaller TKE (Fig. 5b), insufficient representation of the effects of penetrative convection, and less entrainment, thus resulting in the slower growth of the convective ABL (Figs. 3b and 4b). The better performance of the MYNN model relies mainly on the better formulation of L that realistically increases with decreasing stability.

In the lower part of the ABL except near the surface, L in NN30 and NN25 becomes larger than that in the LES, as the ABL develops. This matter will be discussed in the following section. Near the top of the ABL, L in NN25 decreases more rapidly with increasing height than that in NN30. This is because NN25 does not reproduce the weakly stable stratification in the upper half of the ABL (Fig. 3c) and thus the length scale L_B in Eq. (55) does not work for NN25 except above the top of the ABL.

d. *Specific humidity*

Figure 8 shows vertical profiles of specific humidity from the three one-dimensional models and the LES. As the ABL develops, the specific humidity increases (decreases) in the upper (lower) part of the ABL. NN30 predicts these features very well (Fig. 8a). Because of the smaller depth of the ABL, the specific humidity within the ABL in MY30 is about 0.3–0.4 g kg^{-1} larger than that in the LES (Fig. 8b). NN25 has performance comparable to NN30 (Fig. 8c).

Figure 9 shows vertical profiles of moisture flux. The significant negative moisture flux near the top of the ABL in the LES may be an artifact caused by the centered difference scheme of second-order accuracy for the advection term (cf., Moeng 1986), so that the differences of the moisture flux among the models in this region will not be discussed. The profiles after 1200 LST illustrate that the moisture flux increases gradually from the surface to the ABL top and then decreases sharply across the

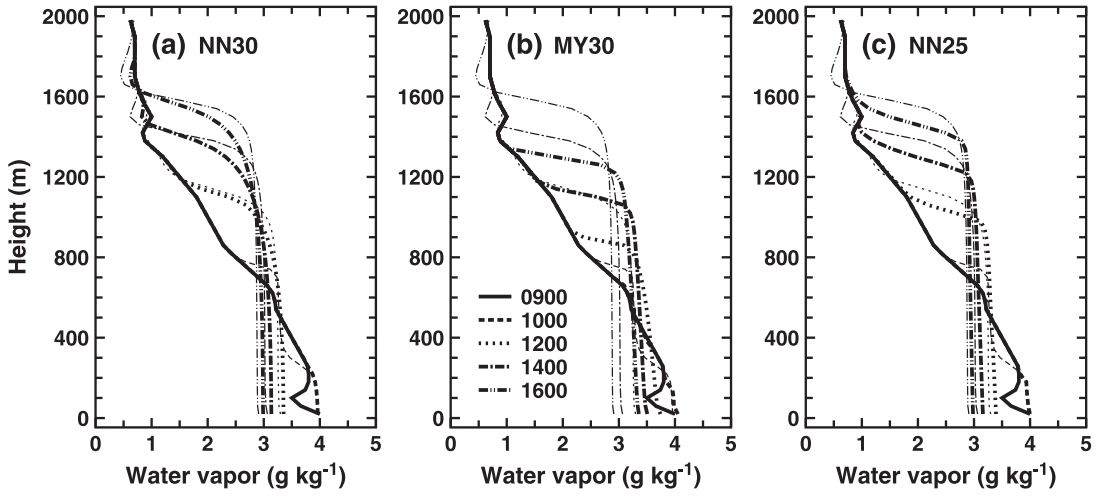

Fig. 8. Same as Fig. 3 but for the specific humidity.

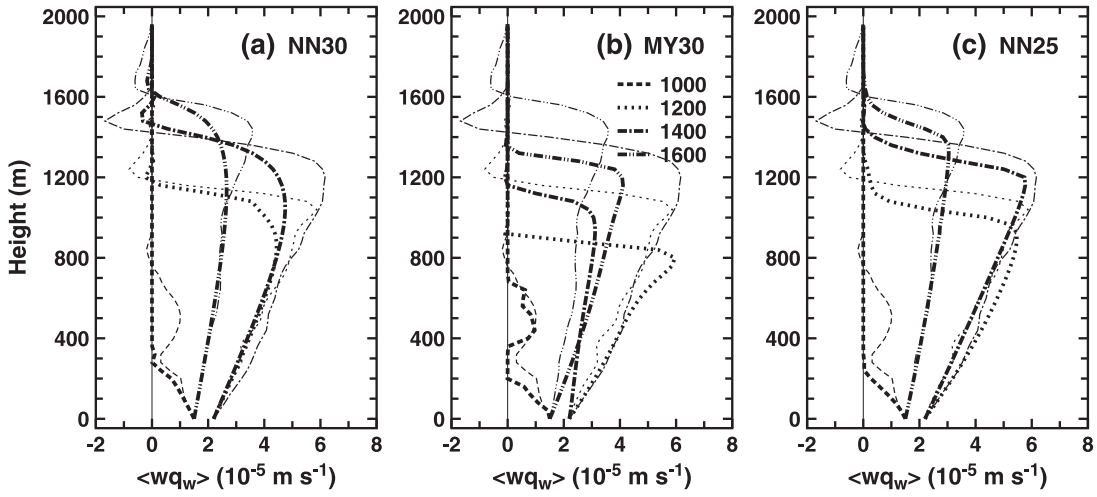

Fig. 9. Same as Fig. 3 but for the vertical moisture flux $\langle wq_w \rangle$.

ABL top. NN30 reproduces generally well the LES results (Fig. 9a). MY30 does not predict the moisture flux very well, particularly at 1400 LST (Fig. 9b). It predicts the flux in the residual layer (between 300 and 700 m) at 1000 LST, although the effect of this flux does not appear clearly to the distribution of the specific humidity (Fig. 8b). The moisture flux near the top of the ABL after 1400 LST in NN25 seems to give slightly better agreement with the LES results than that in NN30 (Fig. 9c). We think that this better agreement for NN25 is rather accidental, since NN25 does not reproduce the weakly stable layer and the effect of L_B in the upper half of the ABL (Fig. 3c).

5. Summary and discussion

Starting from N01, we have made efforts toward improving the MY model. We consider buoyancy effects on the pressure-strain and pressure-temperature-gradient covariances that are neglected in the MY model, and have proposed a new diagnostic equation for the turbulent length scale L that changes realistically with stability. The closure and empirical constants have been determined from the LES database of dry ABLs under different stratifications. We also introduced a partial condensation scheme of Sommeria and Deardorff (1977) and Mellor (1977), and proposed a convenient

computational scheme for a level-3 model (NN04; NN06). This scheme enabled the use of the improved MY (MYNN) level-3 model in an operational weather prediction model of the Japan Meteorological Agency (Hara 2007; Saito et al. 2007).

Although the closure constants are based on our LES database, they have been slightly revised by referring to several recent studies on turbulence closure models. This leads to the following further improvements: The value of C_3 on the buoyancy term in the pressure-temperature-gradient covariance falls within the range of generally accepted values; The stability functions now show better agreement with our LES data (Fig. 1); Finally, the critical gradient Richardson number Ri_c of 0.95 approaches unity, which is the value suggested by a variety of data (cf., Cheng et al. 2002, 2003), although the value of Ri_c is still under some debate.

The good performance of the MYNN model has been demonstrated against a LES of a convective ABL observed on Day 33 of the Wangara experiment (Clarke et al. 1971). Both the MYNN level-3 and level-2.5 models are shown to reproduce fairly well the vertical distributions of the mean and turbulent quantities obtained from the LES, and greatly improve several weak points of the MY model. The level-3 model has the remarkable capability of expressing the countergradient diffusion in the upper part of the ABL (Figs. 3a and 4a), while the level-2.5 model has advantages of diagnostic determination of scalar variances and relatively low computational cost.

The good performance of the MYNN model relies partly on the improvement of the stability functions S_M and S_H for momentum and heat, respectively, through the parameterization of the pressure covariances that includes buoyancy effects (Figs. 1 and 2), and partly on the expression for the stability functions S_q, $S_{\theta l}$, $S_{\theta q}$, and S_{qw} for the third-order turbulent fluxes through S_M (Figs. 5 and 6). The major improvement in its performance, however, is due to our formulation of the turbulent length scale L that realistically increases with decreasing stability (Fig. 7).

For highly unstable stratification, however, the present diagnostic equation for L tends to predict L somewhat larger than that from the LES in the lower part of the ABL except near the surface. Also there is a report that the present diagnostic equation often predicts a somewhat large length scale in the free atmosphere, when it is incorporated into an atmospheric general circulation model (Chikira 2008, personal communication). Note that the present diagnostic model is primarily designed to evaluate L within or right above the ABL. We will continue to examine the applicability to various atmospheric phenomena and, if necessary, make further improvement, while comparing with a number of simulations and observations.

Our formulation of L is essentially based on the LES database of dry ABLs (N01). Therefore it does not explicitly consider the increase or decrease of L accompanying the phase change of water, although the phase change affects the TKE through the buoyancy production and also L indirectly. With the foregoing application to various situations in mind, a more desirable approach may be to develop a prognostic equation for L. Unlike the equation for the TKE, however, an equation for a length scale has little physical basis; i.e., all the turbulent correlation terms that appear in a length scale equation have been parameterized in an analogous way to the corresponding terms in the TKE equation. Furthermore, the prognostic variable has been selected rather arbitrarily; e.g., q^2L was used by Mellor and Yamada (1982) and $q^3/L \sim \varepsilon$ by Hanjalic and Launder (1972). In fact, it is reported that, when the prognostic equation for q^2L proposed by Mellor and Yamada (1982) is used to describe the variation of the length scale with stability in the surface layer, the characteristics of the surface layer including dimensionless shear, dimensionless temperature gradient, and second-order moments are not reproduced for typical range of the dimensionless height $\zeta = z/L_M$ (Niino 1990). Recently, Kantha (2004) formulated a general equation for q^mL^n, where m and n are integer values. We also plan to utilize our diagnostic equation for L for exploring a suitable variable among q^mL^n and empirical constants in its prognostic equation.

Acknowledgements

The present study was performed through Research Revolution 2002 (RR2002) of Project for Sustainable Coexistence of Human, Nature and the Earth of the MEXT of the Japanese Government, and was partly supported by Grant-in-Aids for Scientific Research (B)(2) No. 21340134, the Japan Society for the Promotion of Science. A sample program of the MYNN model is available at http://www.nda.ac.jp/~naka/MYNN/.

Appendix A

Level-2 model

In the level-2 model (Mellor and Yamada 1974, 1982), all the second-order turbulent quantities are calculated diagnostically by neglecting the time-tendency, advection, and diffusion terms.

The diagnostic equation for the TKE is expressed as

$$\begin{aligned} 1 &= B_1(S_{M2}G_M + S_{H2}G_H) \\ &= B_1 S_{M2} G_M(1 - \mathrm{Rf}), \end{aligned} \tag{A1}$$

and gives

$$q_2^2 = B_1 L^2 S_{M2}(1 - \mathrm{Rf})\left[\left(\frac{\partial U}{\partial z}\right)^2 + \left(\frac{\partial V}{\partial z}\right)^2\right], \tag{A2}$$

where S_{M2} and S_{H2} are the stability functions for the level-2 model, Rf the flux Richardson number, and $q_2^2/2$ the TKE per unit mass for the level-2 model. Substitution of Eq. (A1) into Eqs. (27) and (28) gives

$$S_{M2} = \frac{A_1 F_1}{A_2 F_2}\frac{R_{f1} - \mathrm{Rf}}{R_{f2} - \mathrm{Rf}} S_{H2}, \tag{A3}$$

$$S_{H2} = 3A_2(\gamma_1 + \gamma_2)\frac{\mathrm{Rf}_c - \mathrm{Rf}}{1 - \mathrm{Rf}}, \tag{A4}$$

where $\gamma_1 = 0.235$,

$$\gamma_2 = \frac{2A_1(3 - 2C_2) + B_2(1 - C_3)}{B_1}, \tag{A5}$$

$$\begin{aligned} F_1 = {} & B_1(\gamma_1 - C_1) + 2A_1(3 - 2C_2) \\ & + 3A_2(1 - C_2)(1 - C_5), \end{aligned} \tag{A6}$$

$$F_2 = B_1(\gamma_1 + \gamma_2) - 3A_1(1 - C_2), \tag{A7}$$

$$R_{f1} = B_1\frac{\gamma_1 - C_1}{F_1}, \tag{A8}$$

$$R_{f2} = B_1\frac{\gamma_1}{F_2}, \tag{A9}$$

and Rf_c is the critical flux Richardson number given by

$$\mathrm{Rf}_c = \frac{\gamma_1}{\gamma_1 + \gamma_2}. \tag{A10}$$

Unlike the stability functions $S_{M2.5}$ and $S_{H2.5}$ for the level-2.5 model, S_{M2} and S_{H2} are independent of histories of q^2 and L, which appear in G_M and G_H (Eqs. 39 and 40).

The flux Richardson number Rf is obtained from the gradient Richardson number $\mathrm{Ri} \equiv -G_H/G_M = \mathrm{Rf}S_{M2}/S_{H2}$ as

$$\mathrm{Rf} = R_{i1}[\mathrm{Ri} + R_{i2} - (\mathrm{Ri}^2 - R_{i3}\mathrm{Ri} + R_{i2}^2)^{1/2}], \tag{A11}$$

where

$$R_{i1} = \frac{1}{2}\frac{A_2 F_2}{A_1 F_1}, \tag{A12}$$

$$R_{i2} = \frac{1}{2}\frac{R_{f1}}{R_{i1}}, \tag{A13}$$

$$R_{i3} = \frac{2R_{f2} - R_{f1}}{R_{i1}}. \tag{A14}$$

Appendix B

Partial-condensation scheme

Following Sommeria and Deardorff (1977) and Mellor (1977), partial condensation scheme is adopted for the condensation process. We assume the probability distribution of physical quantities around their ensemble averages to be a Gaussian distribution. The liquid-water content Q_l is then given by

$$Q_l = 2\sigma_s\left[RQ_1 + \frac{1}{\sqrt{2\pi}}\exp\left(-\frac{Q_1^2}{2}\right)\right], \tag{B1}$$

where R is the cloud fraction given by

$$R = \frac{1}{2}\left[1 + \mathrm{erf}\left(\frac{Q_1}{\sqrt{2}}\right)\right], \tag{B2}$$

$$\sigma_s^2 = \frac{a^2}{4}\left(\langle q_w^2\rangle - 2b\langle\theta_l q_w\rangle + b^2\langle\theta_l^2\rangle\right), \tag{B3}$$

$$Q_1 = \frac{a(Q_w - Q_{sl})}{2\sigma_s}, \tag{B4}$$

$$a = \left(1 + \frac{L_v}{c_p}\delta Q_{sl}\right)^{-1}, \tag{B5}$$

$$b = \frac{T}{\Theta}\delta Q_{sl}. \tag{B6}$$

$Q_{sl} \equiv Q_s(T_l)$ and $\delta Q_{sl} \equiv \partial Q_s/\partial T|_{T=T_l}$ are determined from the Tetens formula and the Clausius–Clapeyron equation, respectively, where Q_s is the saturation specific humidity and $T_l = \Theta_l T/\Theta$. For the level-2.5 model, Eq. (B3) can be rewritten as

$$\sigma_s^2 = \frac{a^2 L^2 \alpha_c B_2 S_{H2.5}}{4}\left(\frac{\partial Q_w}{\partial z} - b\frac{\partial \Theta_l}{\partial z}\right)^2. \tag{B7}$$

The buoyancy flux $\langle w\theta_V \rangle$ is obtained as

$$\langle w\theta_V \rangle = \beta_\theta \langle w\theta_l \rangle + \beta_q \langle wq_w \rangle, \tag{B8}$$

where

$$\beta_\theta = 1 + 0.61Q_w - 1.61Q_l - \tilde{R}abc, \tag{B9}$$

$$\beta_q = 0.61\Theta + \tilde{R}ac, \tag{B10}$$

$$\tilde{R} = R - \frac{Q_l}{2\sigma_s} \frac{1}{\sqrt{2\pi}} \exp\left(-\frac{Q_1^2}{2}\right), \tag{B11}$$

$$c = (1 + 0.61Q_w - 1.61Q_l)\frac{\Theta}{T}\frac{L_v}{c_p} - 1.61\Theta \tag{B12}$$

(Mellor and Yamada 1982).

References

Abdella, K., and N. McFarlane, 1997: A new second-order turbulence closure scheme for the planetary boundary layer. *J. Atmos. Sci.*, **54**, 1850–1867.

André, J. C., G. De Moor, P. Lacarrère, G. Therry, and R. du Vachat, 1978: Modeling the 24-hour evolution of the mean and turbulent structures of the planetary boundary layer. *J. Atmos. Sci.*, **35**, 1861–1883.

Andrén, A., 1995: The structure of stably stratified atmospheric boundary layers: A large-eddy simulation study. *Quart. J. Roy. Meteor. Soc.*, **121**, 961–985.

Bougeault, P., and P. Lacarrère, 1989: Parameterization of orography-induced turbulence in a mesobeta-scale model. *Mon. Wea. Rev.*, **117**, 1872–1890.

Busch, N. E., and S. E. Larsen, 1972: Spectra of turbulence in the atmospheric surface layer. Risø Report No. 256, Risø National Laboratory, Denmark, 187–207.

Businger, J. A., J. C. Wyngaard, Y. Izumi, and E. F. Bradley, 1971: Flux-profile relationships in the atmospheric surface layer. *J. Atmos. Sci.*, **28**, 181–189.

Canuto, V. M., F. Minotti, C. Ronchi, and R. M. Ypma, 1994: Second-order closure PBL model with new third-order moments: Comparison with LES data. *J. Atmos. Sci.*, **51**, 1605–1618.

Cheng, Y., V. M. Canuto, and A. M. Howard, 2002: An improved model for the turbulent PBL. *J. Atmos. Sci.*, **59**, 1550–1565.

Cheng, Y., V. M. Canuto, and A. M. Howard, 2003: Comments on "On an improved model for the turbulent PBL". *J. Atmos. Sci.*, **60**, 3043–3046.

Cheng, Y., V. M. Canuto, and A. M. Howard, 2005: Nonlocal convective PBL model based on new third- and fourth-order moments. *J. Atmos. Sci.*, **62**, 2189–2204.

Chikira, M., and T. Mochizuki, 2007: Introduction of an improved Mellor–Yamada scheme into MIROC3.2. *Preprints, Autumn Meeting of the Meteorological Society of Japan*, 14–16 October 2007, Sapporo, Japan, 71 pp (in Japanese).

Clarke, R. H., A. J. Dyer, R. R. Brook, D. G. Reid, and A. J. Troup, 1971: The Wangara experiment: Boundary layer data. Technical Paper No. 19, Division of Meteorological Physics, CSIRO, Australia, 358 pp.

Deardorff, J. W., 1972: Theoretical expression for the countergradient vertical heat flux. *J. Geophys. Res.*, **77**, 5900–5904.

Deardorff, J. W., 1974: Three-dimensional numerical study of the height and mean structure of a heated planetary boundary layer. *Bound. Layer Meteor.*, **7**, 81–106.

Deardorff, J. W., 1980: Stratocumulus-capped mixed layers derived from a three-dimensional model. *Bound. Layer Meteor.*, **18**, 495–527.

Galperin, B., L. H. Kantha, S. Hassid, and A. Rosati, 1988: A quasi-equilibrium turbulent energy model for geophysical flows. *J. Atmos. Sci.*, **45**, 55–62.

Gambo, K., 1978: Notes on the turbulence closure model for atmospheric boundary layers. *J. Meteor. Soc. Japan*, **56**, 466–480.

Gerrity, J. P., T. L. Black, and R. E. Treadon, 1994: The numerical solution of the Mellor–Yamada level 2.5 turbulent kinetic energy equation in the eta model. *Mon. Wea. Rev.*, **122**, 1640–1646.

Gibson, M. M., and B. E. Launder, 1978: Ground effects on pressure fluctuations in the atmospheric boundary layer. *J. Fluid Mech.*, **86**, 491–511.

Golaz, J. -C., V. E. Larson, and W. R. Cotton, 2002: A PDF-based model for boundary layer clouds. Part II: Model results. *J. Atmos. Sci.*, **59**, 3552–3571.

Hanjalic, K., and B. E. Launder, 1972: A Reynolds stress model of turbulence and its application to thin shear flows. *J. Fluid Mech.*, **52**, 609–638.

Hara, T., 2007: Update of the operational JMA mesoscale model and implementation of improved Mellor–Yamada level 3 scheme. *Extended Abstracts, 22nd Conf. on Weather Analysis and Forecasting/18th Conf. on Numerical Weather Prediction*, Utah, USA, J3.5.

Helfand, H. M., and J. C. Labraga, 1988: Design of a nonsingular level 2.5 second-order closure model for the prediction of atmospheric turbulence. *J. Atmos. Sci.*, **45**, 113–132.

Hong, S. -Y., Y. Noh, and J. Dudhia, 2006: A new vertical diffusion package with an explicit treatment of entrainment processes. *Mon. Wea. Rev.*, **134**, 2318–2341.

Janjić, Z. I., 2002: Nonsingular implementation of the Mellor–Yamada level 2.5 scheme in the NCEP meso model. Office Note No. 437, National Centers for Environmental Prediction, USA, 61 pp.

Kantha, L. H., 2004: The length scale equation in turbulence models. *Nonlinear Processes Geophys.*, **11**, 83–97.

Kantha, L. H., and C. A. Clayson, 1994: An improved mixed layer model for geophysical applications. *J. Geophys. Res.*, **99**, 25235–25266.

Kiehl, J. T., and K. E. Trenberth, 1997: Earth's annual global mean energy budget. *Bull. Amer. Meteor. Soc.*, **78**, 197–208.

Mellor, G. L., 1973: Analytic prediction of the properties of stratified planetary surface layers. *J. Atmos. Sci.*, **30**, 1061–1069.

Mellor, G. L., 1977: The Gaussian cloud model relations. *J. Atmos. Sci.*, **34**, 356–358. (Corrigenda, 1977: *J. Atmos. Sci.*, **34**, 1483–1484.)

Mellor, G. L., and T. Yamada, 1974: A hierarchy of turbulence closure models for planetary boundary layers. *J. Atmos. Sci.*, **31**, 1791–1806.

Mellor, G. L., and T. Yamada, 1982: Development of a turbulence closure model for geophysical fluid problems. *Rev. Geophys. Space Phys.*, **20**, 851–875.

Moeng, C. -H., 1986: Large-eddy simulation of a stratus-topped boundary layer. Part I: Structure and budgets. *J. Atmos. Sci.*, **43**, 2886–2900.

Moeng, C. -H., and P. P. Sullivan, 1994: A comparison of shear- and buoyancy-driven planetary boundary layer flows. *J. Atmos. Sci.*, **51**, 999–1022.

Moeng, C. -H., and J. C. Wyngaard, 1986: An analysis of closures for pressure-scalar covariances in the convective boundary layer. *J. Atmos. Sci.*, **43**, 2499–2513.

Moeng, C. -H., and J. C. Wyngaard, 1989: Evaluation of turbulent transport and dissipation closures in second-order modeling. *J. Atmos. Sci.*, **46**, 2311–2330.

Nakanishi, M., 2000: Large-eddy simulation of radiation fog. *Bound. Layer Meteor.*, **94**, 461–493.

Nakanishi, M., 2001: Improvement of the Mellor–Yamada turbulence closure model based on large-eddy simulation data. *Bound. Layer Meteor.*, **99**, 349–378.

Nakanishi, M., and H. Niino, 2004: An improved Mellor–Yamada level-3 model with condensation physics: Its design and verification. *Bound. Layer Meteor.*, **112**, 1–31.

Nakanishi, M., and H. Niino, 2006: An improved Mellor–Yamada level-3 model: Its numerical stability and application to a regional prediction of advection fog. *Bound. Layer Meteor.*, **119**, 397–407.

Niino, H., 1990: On the prognostic equation for the turbulent master length scale in a turbulence closure model. *Preprints, Spring Meeting of the Meteorological Society of Japan*, 23–25 May 1990, Tokyo, Japan, 215 pp (in Japanese).

Saito, K., J. Ishida, K. Aranami, T. Hara, T. Segawa, M. Narita, and Y. Honda, 2007: Nonhydrostatic atmospheric models and operational development at JMA. *J. Meteor. Soc. Japan*, **85B**, 271–304.

Schmidt, H., and U. Schumann, 1989: Coherent structure of the convective boundary layer derived from large-eddy simulations. *J. Fluid Mech.*, **200**, 511–562.

Sommeria, G., and J. W. Deardorff, 1977: Subgrid-scale condensation in models of nonprecipitating clouds. *J. Atmos. Sci.*, **34**, 344–355.

Sullivan, P. P., J. C. McWilliams, and C. -H. Moeng, 1994: A subgrid-scale model for large-eddy simulation of planetary boundary-layer flows. *Bound. Layer Meteor.*, **71**, 247–276.

Sun, W. -Y., and Y. Ogura, 1980: Modeling the evolution of the convective planetary boundary layer. *J. Atmos. Sci.*, **37**, 1558–1572.

Therry, G., and P. Lacarrère, 1983: Improving the eddy kinetic energy model for planetary boundary layer description. *Bound. Layer Meteor.*, **25**, 63–88.

Troen, I., and L. Mahrt, 1986: A simple model of the atmospheric boundary layer; sensitivity to surface evaporation. *Bound. Layer Meteor.*, **37**, 129–148.

Turton, J. D., and R. Brown, 1987: A comparison of a numerical model of radiation fog with detailed observations. *Quart. J. Roy. Meteor. Soc.*, **113**, 37–54.

Wyngaard, J. C., and O. R. Coté, 1974: The evolution of a convective planetary boundary layer—A higher-order-closure model study. *Bound. Layer Meteor.*, **7**, 289–308.

Yamada, T., 1977: A numerical experiment on pollutant dispersion in a horizontally-homogeneous atmospheric boundary layer. *Atmos. Environ.*, **11**, 1015–1024.

Yamada, T., and G. L. Mellor, 1975: A simulation of the Wangara atmospheric boundary layer data. *J. Atmos. Sci.*, **32**, 2309–2329.